Revision 1

SiC-dominated ultra-reduced mineral assemblage in carbonatitic xenoliths from the Dalihu basalt, Inner Mongolia, China

Detao He, Yongsheng Liu*, Changgui Gao, Chunfei Chen, Zhaochu Hu, Shan Gao

State Key Laboratory of Geological Processes and Mineral Resources, School of Earth Sciences, China University of Geosciences, Wuhan 430074, China

Words: 7209

Figures: 7

Tables: 2

***Corresponding author**

Yongsheng Liu

State Key Laboratory of Geological Processes and Mineral Resources, China University of Geosciences, Wuhan 430074, China

E-mail: yshliu@hotmail.com or yshliu@cug.edu.cn

Tel: 86-27-87483044

Fax: 86-27-67885096

This is a preprint, the final version is subject to change, of the American Mineralogist (MSA)
Cite as Authors (Year) Title. American Mineralogist, in press.
(DOI will not work until issue is live.) DOI: http://dx.doi.org/10.2138/am-2017-5721

Abstract

SiC and associated ultra-reduced minerals were reported in various geological settings, however, their genesis and preservation mechanism are poorly understood. Here, we reported a SiC dominated ultra-reduced mineral assemblage, including SiC, TiC, native metals (Si, Fe and Ni) and iron silicide, from carbonatitic xenoliths in Dalihu, Inner Mongolia. All minerals were identified in-situ in polished/thin sections. SiC is 20-50 μm in size, blue to colorless in color, and usually identified in the micro-cavities within the carbonatitic xenolith. Four types of SiC polytypes were identified, which are dominated by β-SiC (3C polytype) and 4H polytype followed by 15R and 6H. These SiC are featured by ^{13}C-depleted isotopic compositions ($\delta^{13}C$ = -13.2‰ to - 22.8‰, average = -17.7‰) with obvious spatial variation.

We provided a numerical modeling method to prove that the C isotopic composition of the Dalihu SiC can be well-yielded by degassing. Our modeling results showed that degassing reaction between graphite and silicate can readily produce the low $\delta^{13}C$ value of SiC, and the spatial variations in C isotopic composition could have been formed in the progressive growth process of SiC. The detailed in-situ occurring information is beneficial for our understanding of the preservation mechanism of the Dalihu ultra-reduced phase. The predominant occurrence of SiC in micro-cavities implies that exsolution and filling of CO_2 and/or CO in the micro-cavities during the diapir rising process of carbonatitic melt could have buffered the reducing environment and separated SiC from the surrounding oxidizing phases. The fast cooling of host rock, which would leave insufficient time for the complete elimination of SiC, could have also contributed to the preservation of SiC.

40 **Keywords:** carbonatitic xenolith, silicon carbide, iron silicide, native metal, C isotopic
41 composition

This is a preprint, the final version is subject to change, of the American Mineralogist (MSA)
Cite as Authors (Year) Title. American Mineralogist, in press.
(DOI will not work until issue is live.) DOI: http://dx.doi.org/10.2138/am-2017-5721

Introduction

Natural silicon carbide (SiC) was first reported in the Canyon Diablo meteorite by French chemist Moissan, after whom the material was named as moissanite in 1904. Since then, SiC was discovered in various rocks, including kimberlites (Mathez et al., 1995; Shiryaev et al., 2011), dunite (Liang et al., 2014), tuff (Mukhin et al., 2015), volcanic breccias (Di Pierro et al., 2003), chromitite pods within ophiolites (Trumbull et al., 2009; Xu et al., 2015; Yang et al., 2015), metasedimentary crustal rocks (Janák et al., 2015) and serpentinite in the ultrahigh-pressure (UHP) metamorphic belt (Xu et al., 2008). However, the natural occurrence of SiC has been challenged scientifically for a long time because contamination issues arise from carborundum which is widely used in the geological lab as cutting and abrasion material (Milton and Vitaliano, 1985). Although SiC inclusions in diamond from the Fuxian kimberlite confirm that SiC occurs naturally (Leung et al., 1990; Leung, 1990), SiC is still an enigma mineral in terms of its genesis and its ^{13}C-depleted isotopic composition. Natural SiC always occurs alongside with other reduced phases. SiC can have Si (Di Pierro et al., 2003; Robinson et al., 2004; Shiryaev et al., 2011; Trumbull et al., 2009; Xu et al., 2008), $FeSi_2$ (Shiryaev et al., 2011), Fe_3Si_7 (Di Pierro et al., 2003; Mathez et al., 1995; Robinson et al., 2004) as inclusions and can be accompanied by native Fe and Ni (Fang et al., 2013; Xu et al., 2015) in terrestrial rock. These phases usually require highly reduced conditions, implying that SiC can also be formed under highly reduced environmental conditions. This assumption is strongly supported by high-pressure and high-temperature experiments (high P-T) (Schmidt et al., 2014; Ulmer et al., 1998) and thermodynamic calculations (Mathez et al., 1995), the results of which showed that SiC forms under oxygen fugacities 4 to 9 log

65 units below iron-wustite (IW) buffer. That is an extremely reduced environment,
66 considering that even under the lower mantle, the fO_2 only spans a quite narrow range of
67 values between IW and IW -1.5 (Frost and McCammon, 2008). SiC is strongly depleted
68 in ^{13}C with $\delta^{13}C$ values ranging from -18.2‰ to -34.7‰ (Di Pierro et al., 2003; Leung et
69 al., 1990; Mathez et al., 1995; Trumbull et al., 2009).

70 In this study, we report a new discovery of a SiC-dominated mineral assemblage in
71 carbonatitic xenoliths carried by the Neogene basalt from Dalihu, Inner Mongolia (Gao
72 and Liu, 2008; Liu et al., 2015). These carbonatitic xenoliths offer a rare example of deep
73 mantle recycling of sedimentary carbonate with little altered limestone chemical
74 composition (Liu et al., 2015). Here, we provide a detailed investigation using
75 microanalysis techniques including SIMS, Laser Raman microspectroscopy and EPMA,
76 and model calculations to elucidate the occurrence of SiC and other phases in carbonatitic
77 xenoliths.

78 **Geologic background and sample collection**

79 The Dalihu Neogene volcanic field is located in the southeastern part of the Central
80 Asian Orogenic Belt (CAOB) and close to the North China Craton (Fig. 1) (Xiao et al.,
81 2015). The study area is composed of the Ondor Sum subduction-accretion complex and
82 the Bainaimiao arc (Xiao et al., 2003) (Fig. 1). They are considered to have resulted from
83 the south subduction of the Paleo-Asian Ocean into the North China Craton (Xiao et al.,
84 2003). The subducted oceanic slab carried the crust material into the mantle, and induced
85 melt–peridotite interaction (Liu et al., 2015; Liu et al., 2012; Liu et al., 2010; Xu, 2002).

86 The volcanic activity began approximately 15 Ma and continued to as recently as
87 0.16-0.19 Ma, with the dominant volcanic activity in the Middle Pliocene to the

Quaternary (Ho et al., 2008). The host volcanic rocks have chemical compositions of Mg-rich alkaline basalt with variable and high volatile and $Na_2O + K_2O$ contents (Liu et al., 2015). In addition to carbonatitic xenoliths we investigated here (Fig. 2), peridotite and pyroxenite xenoliths were also carried by the basalt (Zou et al., 2014).

Sample Description

The Dalihu carbonatitic xenoliths are mainly composed of carbonate, and typical upper mantle minerals were also found (Fig. 2). In the carbonatitic xenoliths, medium to coarse-grained orthopyroxene (Opx), clinopyroxene (Cpx) and calcite are cemented by fine-grained calcite matrix (Fig. 2). The proportions of silicate minerals range from 1.5 vol% to 15 vol%. It is worth noting that abundant irregular blebs/cavities, ranging from micrometers to millimeters in diameter, occur in the carbonatitic xenoliths. The irregularly shaped micro-cavities are approximately 200-300 μm in size (Figs. 3a-b). Crystals of quartz and feldspar were also identified (Fig. 3). Reduced minerals, including SiC, TiC, native metals (Si, Fe and Ni), iron silicide and native carbon (graphite and diamond) were also found in the carbonatitic xenoliths (Fig. 3).

Methods

Sample preparation

Thin sections and polished sections for identifying phases: The carbonatitic xenoliths were pretreated by immersing in mixture of epoxy resin and curing agent in a vacuum environment to cement the minerals. To avoid any possible contamination, only Al_2O_3 abrasive papers were used. The surface of the carbonatitic xenolith was first abraded to approximately 1-2 mm in thickness by coarse Al_2O_3 abrasive papers (100 μm)

to remove any possible exotic phases. Next, fine Al_2O_3 abrasive papers of different sizes were used to polish the sections progressively. **Separating SiC for C isotope**: The SiC grains were hand-picked from the heavy fraction of crushed carbonatitic xenoliths. To avoid contamination with synthetic SiC, the mineral separation procedure was processed in a clean room and we carefully cleaned the crusher.

Mineral identification and measurement

Raman microspectroscopy was employed to identify SiC and to determine the SiC polytypes. The analyses were performed using a Thermo Scientific DXR dispersive Raman micro-spectrometer with a 532 nm Nd-YVO4 laser at the State Key Laboratory of Geological Processes and Mineral Resources, China University of Geosciences, Wuhan (CUG-GPMR) (Xiong et al., 2011). Frequencies of Raman bands were monitored by the 1001 cm^{-1} band of standard polystyrene before and after each measurement, and the band-frequency accuracy was approximately 0.5 cm^{-1}. Other phases were first identified using a Quanta 200 environmental scanning electron microscope and GENSIS energy dispersive spectrometer with an accelerating voltage of 20 kV, filament current of 4.4 nA, and work distance of 11.5 mm at CUG-GPMR. Major element compositions were then determined by a JXA-733 electronic microprobe (EMPA) at CUG-GPMR. Analyses were performed on well-polished thin sections using a 15.0 kV accelerating voltage, a 20 nA beam current and a 1 μm probe beam diameter. Silicates and pure oxides were used as standards for calibration.

The secondary ion mass spectrometry (SIMS) analyses were carried out to analyze the C isotopic composition of SiC with a CAMECA NanoSIMS50L at the Institute of Geology and Geophysics, Chinese Academy of Sciences (IGGCAS). A Cs^+ primary beam

133 with the current of ~120 pA and ~0.6 μm in diameter was used during the measurements.
134 The samples were first pre-sputtered using the beam with a higher intensity of 1 nA for 2-
135 3 min in order to remove the gold coating and stabilize the secondary ion yield. The
136 samples were then analyzed by scanning the primary beam over each area of 10×10 μm^2.
137 The instrument was reconfigured for measurements of ^{12}C and ^{13}C, the secondary ions
138 including $^{12}C^-$ and $^{13}C^-$ were integrated using Faraday Cup (FC) and Electron multiplier
139 (EM) respectively in a multi-collection mode (Lin et al., 2014; Miyahara et al., 2015). A
140 mass resolution of ~6000 (10% definition) was used, which was enough to separate the
141 interference of $H^{12}C$ from ^{13}C. The total analysis time of each measurement was ~150
142 seconds. Instrumental mass fractionation (IMF) and analytical uncertainties were
143 monitored using graphite-1 standard ($\delta^{13}C$ = –33.14 ± 0.15‰) (Lin et al., 2014). The
144 results are reported as $\delta^{13}C$ (=[$(^{13}C/^{12}C)_{sample}/(^{13}C/^{12}C)_{PDB}$)-1]×1000‰, $(^{13}C/^{12}C)_{PDB}$ =
145 0.0112372).

146 **Results**

147 **Carbide and native carbon**

148 SiC and TiC were found both in polished sections and as mineral separates. TiC is
149 near pure in chemical composition with trace Al and Cr (Table 1). SiC crystals are 20-50
150 μm in size, blue to colorless in color, and were usually found in the micro-cavities (Fig.
151 3a). Because the stacking sequences of double atomic plane of Si-C along the *c*-direction
152 are variable, many polytypes of SiC were identified, which can be classified into three
153 groups: cubic (C), hexagonal (H) and rhombohedral (R) (Nakashima and Harima, 1997).
154 Laser Raman spectroscopy analyses indicate that SiC in the Dalihu carbonatitic xenoliths
155 are 3C, 4H, 6H and 15R (Fig. 4). 3C SiC have very simple Raman spectrum with only the

156 folded transverse optical mode (FTO) (792-796) and the folded longitudinal optical mode
157 (FLO) (966-969) (Fig. 4a). Raman frequencies of the folded modes for 4H SiC are 203
158 (folded transverse acoustic (FTA), x=0.5), 266 (FTA, x=1), 782 (FTO, x=0.5), 796 (FTO,
159 x=0) and 964 (longitudinal optical plasmon coupled (LOPC)) (Fig. 4b). Raman
160 frequencies of the folded modes for 6H SiC are 160 (FTA, x=0.33), 763 (FTO, x=1), 782
161 (FTO, x=0.33) and 958 (LOPC) (Fig. 4c). Raman frequencies of the folded modes for
162 15R SiC are 172 (FTA, x=0.4), 254 (FTA, x=0.8), 767 (FTO, x=0.8), 782 (FTO, x=0.4),
163 788 (FTO, x=0) (Fig. 4d). The ratio of SiC polytype is 3C: 4H: 15R: 6H = 3:3:2:1.

164 Native carbon in the carbonatitic xenoliths includes graphite and diamond, both of
165 which were found in the polished sections. Graphite is 10-70 μm in size, black in color
166 (Fig. 3c). Based on the Raman bands, the graphite can be classified into two types, highly
167 ordered graphite and disordered graphite (Liu et al., 2015). One diamond (20 μm) was
168 found within the micro-cavity in a polished section.

169 **Metal and metal alloy**

170 **Native Si, Fe, Ni and Fe-Cr alloy.** Native irons are composed of Fe (>99.2 wt%)
171 and minor amounts of Si (~1.68 wt%) and Mn (~0.36 wt%) (Table 1). The irons'
172 chemical compositions are similar to that reported for terrestrial native iron in ophiolite
173 (Bai et al., 2000; Robinson et al., 2004) and native iron in mantle peridotite (Ishimaru et
174 al., 2009), which also have minor amounts of Si and Mn as impurity. Native nickel is
175 composed of Ni (95.7-98.7 wt%) with minor amounts of Fe (0.16-1.54% wt%) (Table 1).
176 Native silicon is near pure with trace amount of Fe (0.12 wt%) (Table 1), which is similar
177 to the native Si as an inclusion in SiC (Shiryaev et al., 2011).

178 **Silicide.** $(Fe,Ni)_2Si$, Fe_3Si and Fe_3Si_7 were found in the thin sections (Fig. 3e). The

crystallochemical formula of $(Fe,Ni)_2Si$ is $Fe_{1.56}Ni_{0.49}Si_{1.00}$ (Table 1), which is similar to that reported for $(Fe,Ni)_2Si$ from lunar meteorite (Nazarov et al., 2012; Nazarov et al., 2015). The crystallochemical formula of Fe_3Si is $Fe_{2.92}Ni_{0.02}Cr_{0.01}Si_{1.08}$ (Table 1). The crystallochemical formula of Fe_3Si (suessite) is similar to that reported for terrestrial and extraterrestrial Fe_3Si (Keil et al., 1982; Novgorodova et al., 1984). The crystallochemical formula of Fe_3Si_7 is $Fe_{2.86}Ti_{0.19}Ni_{0.16}Al_{0.11}Si_{7.00}$ (Table 1).

C isotopic compositions of SiC

C isotopic compositions of SiC found in the carbonatitic xenoliths feature strong depletion in ^{13}C ($\delta^{13}C$ = -13.2‰ to - 22.8‰) compared to the normal mantle carbon reservoir ($\delta^{13}C$ = ~ -5‰; Deines, 2002) (Table 2, Fig. 5). It has been reported that $\delta^{13}C$ values vary from -28.8‰ to -22.3‰ for SiC from kimberlites (Leung et al., 1990; Mathez et al., 1995), from -23.5‰ to -32.7‰ for SiC from Ophiolite (Trumbull et al., 2009) and from -20.9‰ to -31.0‰ for SiC from the Turkish beach (Di Pierro et al., 2003; Trumbull et al., 2009). These observations imply that SiC in the Dalihu carbonatitic xenoliths are slightly richer in ^{13}C than that from kimberlite and ophiolite (Fig. 5).

Detailed in-situ analyses reveal that the Dalihu SiC are highly heterogeneous in $\delta^{13}C$ value (Table 2), and show two types of $\delta^{13}C$ variation pattern (Fig. 6). $\delta^{13}C$ values of three SiC separates vary significantly across the polished section (e.g., -13.2‰ to -20.8‰ for SiC-2). Although the other three SiC separates show no obvious spatial variation, their $\delta^{13}C$ values are different from each other (Fig. 6, Table 2).

Discussion

Natural occurrence of SiC

Before furthering serious discussion in the natural SiC study field, the contamination problem should be eliminated because carborundum is a widely used material in geological labs. Special sample preparation methods are the key to avoid artificial SiC contamination and to confirm natural SiC occurrence. In this work, a SiC free sample preparation procedure was applied to prepare the polished sections for in-situ identification of the occurrence of SiC, as described in the sample preparation section. Our further analyses indicate that there is also a significant distinction between the Dalihu SiC and synthetic SiC in terms of crystal structure. The Dalihu SiC grains are dominated by β-SiC (3C polytype) and 4H polytype (Fig. 4), while type 6H is dominant volume of commercial production of SiC followed by 15R and 4H with rare 3C (Fisher and Barnes, 1990; Trigunayat and Chadha, 1971; van Loan, 1967). Furthermore, SiC does not occur independently in the Dalihu carbonatitic xenolith, but exists as an ultra-reduced phase assemblage including SiC, TiC, native metals (Si, Fe and Ni) and iron silicide. Such type of mineral assemblages were also reported in kimberlite (Shiryaev et al., 2011) and chromitite pods within ophiolites (Trumbull et al., 2009; Xu et al., 2015; Yang et al., 2015). Collectively, the special sample preparation and experimental observations confirm that the Dalihu SiC in the carbonatitic xenoliths occurs naturally.

Formation mechanism of the ultra-reduced mineral assemblage

Considerable debate has occurred over the origin of SiC, mainly because SiC only formed under extremely reduced conditions (Mathez et al., 1995; Schmidt et al., 2014), and it is strongly depleted in ^{13}C ($\delta^{13}C = -18‰$ to $-35‰$) (Di Pierro et al., 2003; Leung et al., 1990; Mathez et al., 1995; Trumbull et al., 2009). Some researchers suggest that SiC could have originated from a low fO_2 deep mantle domain (Mathez et al., 1995;

Trumbull et al., 2009), formed by recycled organic materials (Schmidt et al., 2014). However, Rodgers et al. (1989) found that the formation of some natural moissanites do not require the very deep mantle conditions. Shiryaev and Gaillard (2014) suggest that the extremely reducing conditions necessary to form SiC can be achieved by reaction between graphite and silicate mineral with CO degassing ($6C+4MgSiO_3 \rightarrow 2SiC+4CO+2Mg_2SiO_4$) during the ultimate steps of ascent of carbon-saturated melts, when pressure is lower than 100 bars. Horita and Polyakov (2015) found that SiC can be significantly depleted in ^{13}C relative to other C-bearing materials even at mantle temperatures, and suggest that $\delta^{13}C$ values of SiC are lower than any other C-bearing mantle phases (diamond, CO_2, CH_4, and $CaCO_3$) by 6–11‰ at 1000°C based on theoretical calculations. These works imply that SiC may also originate from a shallow region with normal C isotopic composition and does not necessarily form in extremely oxygen-depleted regions in the deep mantle.

C isotopic composition of SiC may play an important role in tracing the origin of SiC. SiC crystallized from a deep and reducing mantle region should have homogenous C isotopic composition. However, some SiC grains show remarkable spatial variation in $\delta^{13}C$ value, suggesting that the Dalihu SiC formed in a continuing reaction process, rather than crystallized from a C isotope homogenous reservoir. Primarily, the C isotopic composition of the Dalihu SiC seems to support the degassing origin hypothesis of SiC. Here, we provided a numerical modeling (see Appendix) to prove that SiC can be well yielded by degassing in terms of its low $\delta^{13}C$ value and spatial variation of C isotopic composition (Fig. 7).

Degassing of CO_2 and CO were both involved to create modeling of C isotopic

247 composition of SiC using the reaction formulas $2C+SiO_2 \rightarrow SiC+CO_2$ (Liu et al., 2015)
248 and $6C+4MgSiO_3 \rightarrow 2SiC+4CO+2Mg_2SiO_4$ (Shiryaev and Gaillard, 2014), respectively.
249 The $\delta^{13}C$ value of SiC formed by degassing is mainly controlled by the initial $\delta^{13}C$ value
250 of graphite, the reaction temperature and the extent of reaction. Obviously, SiC that
251 originated from graphite with a high initial $\delta^{13}C$ value would have a higher $\delta^{13}C$ value
252 compared to that originated from graphite with a low initial $\delta^{13}C$ (Fig. 7). The $\delta^{13}C$ value
253 of SiC increases with temperature increasing because the C isotope fractionation becomes
254 small under high temperature (Horita and Polyakov, 2015; Polyakov and Kharlashina,
255 1995; Richet et al., 1977). However, there is still a clear trend that the $\delta^{13}C$ value of the
256 initially formed SiC is the lowest, and increases as the reaction proceeds (Fig. 7). Thus,
257 the SiC formed by degassing would have radical variation in C isotopic composition, as
258 shown by the Dalihu SiC separates (Fig 6).

259 The very low pressure degassing ($6C+4MgSiO_3 \rightarrow 2SiC+4CO+2Mg_2SiO_4$) is only
260 available to produce SiC at high temperature (~1300°C) (Shiryaev and Gaillard, 2014).
261 However, such degassing reaction can't produce SiC with low $\delta^{13}C$ value due to the
262 insignificant C isotope fractionation at high temperature (Fig. 7c) (Horita and Polyakov,
263 2015; Polyakov and Kharlashina, 1995; Richet et al., 1977). Furthermore, no high
264 temperature of >1200°C was recorded by the Dalihu carbonatitic xenoliths (Liu et al.,
265 2015). Therefore, we prefer that the Dalihu SiC could have not been formed by low
266 pressure degassing. SiO_2 saturation is indicated by the presence of quartz and feldspar in
267 the SiC-bearing carbonatitic xenoliths (Figs. 3h-i). Liu et al. (2015) thus suggested that
268 the Dalihu SiC could have been formed by the reaction of $2C+SiO_2 \rightarrow SiC+CO_2$ during
269 the rapid ascent of carbonate-rich diapir from the top of the slab to the shallow mantle

because CO concentration is negligible at pressures ≥1 kbar (Ferry and Baumgartner, 1987). Our numerical modeling shows that the very low $\delta^{13}C$ value of the Dalihu SiC can be readily produced by the degassing reaction of $2C+SiO_2 \rightarrow SiC+CO_2$ at temperature 784–1046 °C (Liu et al., 2015). The spatial variations of C isotopic compositions could have been formed in the progressive growth process of SiC. Santosh et al. (2003) and Satish-Kumar et al. (2011) found that graphite could exhibit unidirectional $\delta^{13}C$ variation along the growth direction, but homogenous $\delta^{13}C$ value perpendicular to the growth direction within a single graphite. The two types of $\delta^{13}C$ variation pattern of the Dalihu SiC (Fig. 6) could result from the direction of profile measurement as well. In other words, SiC profiles parallel to the growth direction show obvious variation of $\delta^{13}C$ value, while SiC profiles perpendicular to growth direction show limited variation of $\delta^{13}C$ value.

The earth mantle is featured by a major C isotopic composition with $\delta^{13}C$ value of about -5‰ (Deines, 2002). However, some mantle materials with ^{13}C-depleted isotopic composition were also reported. For example, eclogitic diamonds and peridotitic diamonds cover a range of $\delta^{13}C$ value from −41.3 to 2.7‰, −26.4 to 0.2‰ respectively, whereas $\delta^{13}C$ values of carbonados vary from −32 to −25‰ and up to −5‰ (Shirey et al., 2013). And almost all of the SiC and iron carbide have very low $\delta^{13}C$ values, ranging from -18.2 to -34.7‰ for SiC (Di Pierro et al., 2003; Leung et al., 1990; Mathez et al., 1995; Trumbull et al., 2009) and -16.9 to -27.5‰ for iron carbide (Mikhail et al., 2014a). These observations seem to indicate that there may be a lot of organic sediments with light carbon recycled into mantle through subduction processes. However, the recycled organic sediments model is challenged due to the thermal stability of organic compounds and the low ratio of organic carbon to carbonate in subduction zones (Cartigny, 2005;

Mikhail et al., 2014b). Another model to explain the low $\delta^{13}C$ value of some mantle materials is C isotope fractionation in degassing reaction. Recently, Horita and Polyakov (2015) well explained the low $\delta^{13}C$ value of diamond by C isotope fractionation using theoretical calculations. Here, our study on the SiC-bearing carbonatitic xenoliths provide natural evidence for the formation of ^{13}C-depleted feature of some mantle materials by C isotope fractionation. We thus speculate that many of the ^{13}C-depleted mantle material may not necessarily indicate recycling of organic sediments.

The preservation of ultra-reduced mineral assemblage

SiC, native metal, iron silicide and carbide are highly reduced minerals. However, they are hosted in the oxidizing rock. Ultra-reduced mineral assemblages hosted in the oxidizing rock are an unexpected discovery because they are considered to be oxidized by surrounding minerals at high temperature. For example, even mm-sized SiC would disappear through diffusive equilibration within a million years at temperatures above 800-900°C (Schmidt et al., 2014). Detailed occurrence information may help us to understand the preservation mechanism of SiC dominated ultra-reduced minerals in the Dalihu carbonatitic xenoliths. Previous studies have mainly focused on separated SiC particles (Mathez et al., 1995; Shiryaev et al., 2011; Trumbull et al., 2009; Xu et al., 2015; Yang et al., 2015) and only several reliable in-situ SiC instances have been reported in serpentinite (Xu et al., 2008), dunite (Liang et al., 2014), metasedimentary crustal rocks (Janák et al., 2015) and tuff (Mukhin et al., 2015), while the original occurrence information, such as occurrence site, surrounding minerals, was lost.

We note that the Fuxian SiC, which occur as inclusions in diamond (Leung et al., 1990; Leung, 1990), may provide us a reasonable clue to revealing the preservation

316 mechanism of SiC in crust- and mantle-derived rocks. Diamond is a stable reduced
317 carbon phase in the deep mantle (Rohrbach and Schmidt, 2011), so SiC wrapped within
318 diamond may survive in mantle due to the protection of the diamond from the oxidizing
319 environment. And the rapid ascent of kimberlite also aids the preservation of diamond
320 and SiC during the transport process (Wilson and Head Iii, 2007). This leads us to
321 speculate that SiC may be preserved in a local reducing buffer in the carbonatitic
322 xenoliths, as well. We found that almost all the in-situ SiC was found within the micro-
323 cavities in the Dalihu carbonatitic xenoliths. The micro-cavities and micro-cracks may
324 result from the exsolution of the volatile phase during the diapir rising process of
325 carbonatitic melt (Liu et al., 2015; Russell et al., 2012). These micro-cavities and micro-
326 cracks can accelerate evacuating CO_2 or CO, and thus promote the reactions forming SiC,
327 which accounts for the preferred occurrence of SiC in the micro-cavities. Furthermore,
328 filling of CO_2 and/or CO in the micro-cavities could have buffered the reducing
329 environment and separated SiC from the surrounding oxidizing phases. On the other
330 hand, the fast cooling of host rock could have also contributed to the preservation of SiC.
331 The heterogeneous C isotopic compositions (Fig. 6) indicate that SiC in the carbonatitic
332 xenoliths were preserved at a relatively low temperature because the $\delta^{13}C$ value would be
333 quickly homogenized at high temperature (Horita and Polyakov, 2015). These
334 observations suggest that the carbonatitic melt once suffered rapid transportation into the
335 shallow lithospheric mantle, cooling just shortly after segregation from the source (Liu et
336 al., 2015) which would leave insufficient time for the complete elimination of SiC.

337 **Implications**

338 SiC and associated minerals have been discussed for a long time; however, SiC

remains a poorly understood mineral. There is still no consensus on the genesis of SiC and the origin of low $\delta^{13}C$ values of SiC. Due to the lack of these basic information, SiC is not a good indicator mineral for geological processes. SiC dominated ultra-reduced mineral assemblages, including SiC, TiC, native metals (Si, Fe and Ni) and iron silicide, were observed in the carbonatitic xenoliths carried by the Neogene basalt in the southeastern part of Central Asian Orogenic Belt. This is a new geologic setting for SiC dominated ultra-reduced phase assemblages.

The SiC reported here are dominated by β-SiC (3C polytype) and 4H polytype followed by 15R and 6H. They feature low and heterogeneous $\delta^{13}C$ values ($\delta^{13}C$ = -13.2‰ to - 22.8‰, average = -17.7‰). Some grains show obvious spatial variation. The low $\delta^{13}C$ value of SiC can be well modeled by a graphite-silicate reaction forming SiC with degassing, which implies an intrinsic property of low $\delta^{13}C$ value rather than being inherited from a ^{13}C-depleted source region. Detailed spatial information on $\delta^{13}C$ value in SiC grains is helpful for tracing the origin of SiC. However, it is still necessary to determine the C isotopic fractionation during graphite-silicate reaction with degassing by high P-T experiments.

The in-situ occurrence of SiC in polished sections provides a great opportunity to understand the preservation mechanism of ultra-reduced phases in an oxidized environment. The wide development of micro-cavities provides not only the channels for degassing of CO_2 or CO and thus promoting the formation of SiC but also buffers the reducing environment and separates SiC from the surrounding oxidizing phases. However, the preservation mechanism of SiC in other geological settings, such as kimberlite and ophiolite, is still unknown. Our research suggests that detailed mapping

362 work to identify SiC in-situ may contribute to the discussion of its preservation
363 mechanism.

364 **Acknowledgments**

365 We thank three anonymous reviewers for their constructive comments which have
366 greatly improved the manuscript. We are grateful to Dr. Wei Yang, Jianchao Zhang for
367 assistance with the SIMS analyses, to Suxin Zhang for assistance with the environmental
368 scanning electron microscope and to Yi Bao, Xianquan Ping for help with the Raman
369 measurements. This research is co-supported by the 973 project (2013CB429806), NSFC
370 (41125013 and 41530211), Specialized Research Fund for the Doctoral Program of
371 Higher Education (20130145110001) and the MOST Special Funds of the State Key
372 Laboratory of Geological Processes and Mineral Resources.

References cited

Bai, W., Robinson, P.T., Fang, Q., Yang, J., Yan, B., Zhang, Z., Hu, X.-F., Zhou, M.-F., and Malpas, J. (2000) The PGE and base-metal alloys in the podiform chromitites of the Luobusa ophiolite, southern Tibet. The Canadian Mineralogist, 38, 585-598.

Cartigny, P. (2005) Stable isotopes and the origin of diamond. Elements, 1, 79-84.

Deines, P. (2002) The carbon isotope geochemistry of mantle xenoliths. Earth-Science Reviews, 58, 247-278.

Deines, P., and Eggler, D.H. (2009) Experimental determination of carbon isotope fractionation between CaCO3 and graphite. Geochimica et Cosmochimica Acta, 73, 7256-7274.

Di Pierro, S., Gnos, E., Grobety, B.H., Armbruster, T., Bernasconi, S.M., and Ulmer, P. (2003) Rock-forming moissanite (natural α-silicon carbide). American Mineralogist, 88, 1817-1821.

Fang, Q., Bai, W., Yang, J., Rong, H., Shi, N., Li, G., Xiong, M., and Ma, Z. (2013) Titanium, Ti, A New Mineral Species from Luobusha, Tibet, China. Acta Geologica Sinica - English Edition, 87, 1275-1280.

Ferry, J.M., and Baumgartner, L. (1987) Thermodynamic models of molecular fluids at the elevated pressures and temperatures of crustal metamorphism. Reviews in Mineralogy and Geochemistry, 17, 323-365.

Fisher, G., and Barnes, P. (1990) Towards a unified view of polytypism in silicon carbide. Philosophical Magazine B, 61, 217-236.

Frost, D.J., and McCammon, C.A. (2008) The redox state of Earth's mantle. Annual

396 Review of Earth and Planetary Sciences, 36, 389-420.
397 Gao, C., and Liu, Y. (2008) Moissanite-Bearing Carbonatite Xenoliths from Cenozoic
398 Basalt, North China: Products of Ancient Oceanic Crust Subduction? Geochimica
399 et Cosmochimica Acta, 72, A292-A292.
400 Ho, K.-S., Liu, Y.A.N., Chen, J.-C., and Yang, H.-J. (2008) Elemental and Sr-Nd-Pb
401 isotopic compositions of late Cenozoic Abaga basalts, Inner Mongolia:
402 Implications for petrogenesis and mantle process. Geochemical Journal, 42, 339-
403 357.
404 Horita, J., and Polyakov, V.B. (2015) Carbon-bearing iron phases and the carbon isotope
405 composition of the deep Earth. Proceedings of the National Academy of Sciences,
406 112, 31-36.
407 Ishimaru, S., Arai, S., and Shukuno, H. (2009) Metal-saturated peridotite in the mantle
408 wedge inferred from metal-bearing peridotite xenoliths from Avacha volcano,
409 Kamchatka. Earth and Planetary Science Letters, 284, 352-360.
410 Janák, M., Froitzheim, N., Yoshida, K., Sasinková, V., Nosko, M., Kobayashi, T.,
411 Hirajima, T., and Vrabec, M. (2015) Diamond in metasedimentary crustal rocks
412 from Pohorje, Eastern Alps: a window to deep continental subduction. Journal of
413 Metamorphic Geology, 33, 495-512.
414 Keil, K., Berkley, J.L., and Fuchs, L.H. (1982) Suessite, Fe3Si, a new mineral in the
415 North Haig ureilite. American Mineralogist, 67, 126-131.
416 Leung, I., Guo, W., Friedman, I., and Gleason, J. (1990) Natural occurrence of silicon
417 carbide in a diamondiferous kimberlite from Fuxian. Nature, 346, 352-354.
418 Leung, I.S. (1990) Silicon carbide cluster entrapped in a diamond from Fuxian, China.

419 American Mineralogist, 75, 1110-1119.
420 Liang, F., Xu, Z., and Zhao, J. (2014) In-situ Moissanite in Dunite: Deep Mantle Origin
421 of Mantle Peridotite in Luobusa Ophiolite, Tibet. Acta Geologica Sinica - English
422 Edition, 88, 517-529.
423 Lin, Y., El Goresy, A., Hu, S., Zhang, J., Gillet, P., Xu, Y., Hao, J., Miyahara, M., Ouyang,
424 Z., Ohtani, E., Xu, L., Yang, W., Feng, L., Zhao, X., Yang, J., and Ozawa, S.
425 (2014) NanoSIMS analysis of organic carbon from the Tissint Martian meteorite:
426 Evidence for the past existence of subsurface organic-bearing fluids on Mars.
427 Meteoritics & Planetary Science, 49, 2201-2218.
428 Liu, Y., He, D., Gao, C., Foley, S., Gao, S., Hu, Z., Zong, K., and Chen, H. (2015) First
429 direct evidence of sedimentary carbonate recycling in subduction-related
430 xenoliths. Sci Rep, 5, 11547.
431 Liu, Y., Wang, X., Wang, D., He, D., Zong, K., Gao, C., Hu, Z., and Gong, H. (2012)
432 Triassic high-Mg adakitic andesites from Linxi, Inner Mongolia: Insights into the
433 fate of the Paleo-Asian ocean crust and fossil slab-derived melt–peridotite
434 interaction. Chemical Geology, 328, 89-108.
435 Liu, Y.S., Gao, S., Hu, Z.C., Gao, C.G., Zong, K.Q., and Wang, D.B. (2010) Continental
436 and Oceanic Crust Recycling-induced Melt-Peridotite Interactions in the Trans-
437 North China Orogen: U-Pb Dating, Hf Isotopes and Trace Elements in Zircons
438 from Mantle Xenoliths. Journal of Petrology, 51, 537-571.
439 Mathez, E., Fogel, R., Hutcheon, I., and Marshintsev, V. (1995) Carbon isotopic
440 composition and origin of SiC from kimberlites of Yakutia, Russia. Geochimica et
441 Cosmochimica Acta, 59, 781-791.

442 Mikhail, S., Guillermier, C., Franchi, I.A., Beard, A.D., Crispin, K., Verchovsky, A.B.,
443 Jones, A.P., and Milledge, H.J. (2014a) Empirical evidence for the fractionation of
444 carbon isotopes between diamond and iron carbide from the Earth's mantle.
445 Geochemistry, Geophysics, Geosystems, 15, 855-866.
446 Mikhail, S., Verchovsky, A.B., Howell, D., Hutchison, M.T., Southworth, R., Thomson,
447 A.R., Warburton, P., Jones, A.P., and Milledge, H.J. (2014b) Constraining the
448 internal variability of the stable isotopes of carbon and nitrogen within mantle
449 diamonds. Chemical Geology, 366, 14-23.
450 Milton, C., and Vitaliano, D. (1985) Moissanite SiC, a geological aberration. 98th Ann.
451 Meeting, The Geological Society of America, Orlando Florida.
452 Miyahara, M., Ohtani, E., El Goresy, A., Lin, Y., Feng, L., Zhang, J.-C., Gillet, P.,
453 Nagase, T., Muto, J., and Nishijima, M. (2015) Unique large diamonds in a
454 ureilite from Almahata Sitta 2008 TC3 asteroid. Geochimica et Cosmochimica
455 Acta, 163, 14-26.
456 Mukhin, P., Eppelbaum, L., Wirth, R., Schreiber, A., and Dobrzhinetskaya, L. (2015)
457 First Find of 4H SiC Polytype in situ in Volcanic Rocks of Northern Israel.
458 Goldschmidt Abstracts, 2205.
459 Nakashima, S., and Harima, H. (1997) Raman Investigation of SiC Polytypes. physica
460 status solidi (a), 162, 39-64.
461 Nazarov, M.A., Demidova, S.I., Anosova, M.O., Kostitsyn, Y.A., Ntaflos, T., and
462 Brandstaetter, F. (2012) Native silicon and iron silicides in the Dhofar 280 lunar
463 meteorite. Petrology, 20, 506-519.
464 Nazarov, M.A., Shornikov, S.I., and Demidova, S.I. (2015) Origin of native silicon and

iron silicides in the Dhofar 280 lunar meteorite. Petrology, 23, 168-175.

Novgorodova, M.I., Yusupov, R.G., Dmitrieva, M.T., Tsepin, A.I., Sivtsov, A.V., Gorshkov, A.I., Korovushkin, V.V., and Yakubovskaya, N.Y. (1984) First Occurrence of Suessite on the Earth. International Geology Review, 26, 98-101.

Polyakov, V.B., and Kharlashina, N.N. (1995) The use of heat capacity data to calculate carbon isotope fractionation between graphite, diamond, and carbon dioxide: a new approach. Geochimica Et Cosmochimica Acta, 59, 2561-2572.

Richet, P., Bottinga, Y., and Javoy, M. (1977) A review of hydrogencarbon, nitrogen, oxygen, sulphur and chlorine stable isotope fractionation among gaseous molecules. Annual Review of Earth and Planetary Sciences, 5, 65-110.

Robinson, P.T., Bai, W.J., Malpas, J., Yang, J.S., Zhou, M.F., Fang, Q.S., Hu, X.F., Cameron, S., and Staudigel, H. (2004) Ultra-high pressure minerals in the Luobusa Ophiolite, Tibet, and their tectonic implications. Geological Society, London, Special Publications, 226, 247-271.

Rodgers, K., Courtney, S., Seelye, R., McCullock, A., and Mulholland, I. (1989) An occurrence of “moissanite”(SiC) from Seddonville, West Coast, New Zealand. New Zealand Natural Sciences, 16, 105-108.

Rohrbach, A., and Schmidt, M.W. (2011) Redox freezing and melting in the Earth's deep mantle resulting from carbon-iron redox coupling. Nature, 472, 209-12.

Russell, J.K., Porritt, L.A., Lavallee, Y., and Dingwell, D.B. (2012) Kimberlite ascent by assimilation-fuelled buoyancy. Nature, 481, 352-6.

Santosh, M., Wada, H., Satish-Kumar, M., and Binu-Lal, S.S. (2003) Carbon isotope “stratigraphy” in a single graphite crystal: Implications for the crystal growth

mechanism of fluid-deposited graphite. American Mineralogist, 88, 1689-1696.

Satish-Kumar, M., Yurimoto, H., Itoh, S., and Cesare, B. (2011) Carbon isotope anatomy of a single graphite crystal in a metapelitic migmatite revealed by high-spatial resolution SIMS analysis. Contributions to Mineralogy and Petrology, 162, 821-834.

Schmidt, M.W., Gao, C., Golubkova, A., Rohrbach, A., and Connolly, J. (2014) Natural moissanite (SiC) – a low temperature mineral formed from highly fractionated ultra-reducing COH-fluids. Progress in Earth and Planetary Science, 1, 27.

Shirey, S.B., Cartigny, P., Frost, D.J., Keshav, S., Nestola, F., Nimis, P., Pearson, D.G., Sobolev, N.V., and Walter, M.J. (2013) Diamonds and the Geology of Mantle Carbon. Reviews in Mineralogy and Geochemistry, 75, 355-421.

Shiryaev, A.A., and Gaillard, F. (2014) Local redox buffering by carbon at low pressures and the formation of moissanite – natural SiC. European Journal of Mineralogy, 26, 53-59.

Shiryaev, A.A., Griffin, W.L., and Stoyanov, E. (2011) Moissanite (SiC) from kimberlites: Polytypes, trace elements, inclusions and speculations on origin. Lithos, 122, 152-164.

Trigunayat, G., and Chadha, G. (1971) Progress in the study of polytypism in crystals (I). physica status solidi (a), 4, 9-42.

Trumbull, R.B., Yang, J.S., Robinson, P.T., Di Pierro, S., Vennemann, T., and Wiedenbeck, M. (2009) The carbon isotope composition of natural SiC (moissanite) from the Earth's mantle: New discoveries from ophiolites. Lithos, 113, 612-620.

Ulmer, G.C., Grandstaff, D.E., Woermann, E., Gobbels, M., Schonitz, M., and Woodland, A.B. (1998) The redox stability of moissanite (SiC) compared with metal-metal oxide buffers at 1773 K and at pressures up to 90 kbar. Neues Jahrbuch Fur Mineralogie-Abhandlungen, 172, 279-307.

van Loan, P.R. (1967) A study of polytypism in silicon carbide. American Mineralogist, 52, 946-956.

Wilson, L., and Head Iii, J.W., 3rd. (2007) An integrated model of kimberlite ascent and eruption. Nature, 447, 53-7.

Xiao, W., Windley, B.F., Hao, J., and Zhai, M. (2003) Accretion leading to collision and the Permian Solonker suture, Inner Mongolia, China: Termination of the central Asian orogenic belt. Tectonics, 22, 1069.

Xiao, W., Windley, B.F., Sun, S., Li, J., Huang, B., Han, C., Yuan, C., Sun, M., and Chen, H. (2015) A Tale of Amalgamation of Three Permo-Triassic Collage Systems in Central Asia: Oroclines, Sutures, and Terminal Accretion. Annual Review of Earth and Planetary Sciences, 43, 477-507.

Xiong, Q., Zheng, J., Griffin, W.L., O'Reilly, S.Y., and Zhao, J. (2011) Zircons in the Shenglikou ultrahigh-pressure garnet peridotite massif and its country rocks from the North Qaidam terrane (western China): Meso-Neoproterozoic crust–mantle coupling and early Paleozoic convergent plate-margin processes. Precambrian Research, 187, 33-57.

Xu, S., Wu, W., Xiao, W., Yang, J., Chen, J., Ji, S., and Liu, Y. (2008) Moissanite in serpentinite from the Dabie Mountains in China. Mineralogical Magazine, 72, 899-908.

534 Xu, X., Yang, J., Robinson, P.T., Xiong, F., Ba, D., and Guo, G. (2015) Origin of
535 ultrahigh pressure and highly reduced minerals in podiform chromitites and
536 associated mantle peridotites of the Luobusa ophiolite, Tibet. Gondwana
537 Research, 27, 686-700.
538 Xu, Y. (2002) Evidence for crustal components in the mantle and constraints on crustal
539 recycling mechanisms: pyroxenite xenoliths from Hannuoba, North China.
540 Chemical Geology, 182, 301-322.
541 Yang, J., Meng, F., Xu, X., Robinson, P.T., Dilek, Y., Makeyev, A.B., Wirth, R.,
542 Wiedenbeck, M., and Cliff, J. (2015) Diamonds, native elements and metal alloys
543 from chromitites of the Ray-Iz ophiolite of the Polar Urals. Gondwana Research,
544 27, 459-485.
545 Zou, D., Liu, Y., Hu, Z., Gao, S., Zong, K., Xu, R., Deng, L., He, D., and Gao, C. (2014)
546 Pyroxenite and peridotite xenoliths from Hexigten, Inner Mongolia: Insights into
547 the Paleo-Asian Ocean subduction-related melt/fluid–peridotite interaction.
548 Geochimica et Cosmochimica Acta, 140, 435-454.

549 **Figure captions:**

550 Figure 1. Tectonic sketch map of the study area modified after Xiao et al. (2003).

551 Figure 2. **(a)** Field appearance of the carbonatitic xenolith. **(b)** Section of one carbonatitic
552 xenolith. **(c,d)** Pyroxenes in the carbonatitic xenolith.

553 Figure 3. **(a)** Optical and **(b)** backscattered electron images of SiC in the micro-cavity. **(c)**
554 Optical image of in-situ graphite in the micro-cavity. **(d)** Backscattered electron image of
555 separated TiC. **(e)** Backscattered electron image of Fe_3Si coexisting with SiC. **(f)**
556 Backscattered electron image of native Ni. **(g)** Backscattered electron image of native Fe.
557 **(h)** Backscattered electron image of feldspar. **(i)** Backscattered electron image of quartz.

558 Figure 4. Raman spectrums of SiC grains.

559 Figure 5. Stacked histogram of $\delta^{13}C$ value of SiC from different settings. SiC grains in
560 kimberlite (Mathez et al., 1995), SiC inclusion in diamond (Leung et al., 1990), rock-
561 forming SiC from Turkish beach (Di Pierro et al., 2003; Trumbull et al., 2009) and SiC
562 separated from podiform chromitites from Ray-Iz, Luobusa, Dongqiao and Semail
563 ophiolites (Trumbull et al., 2009) are shown for comparison.

564 Figure 6. Profile variations of $\delta^{13}C$ value of SiC grains. $\delta^{13}C$ value of the bulk
565 carbonatitic xenolith is shown for comparison.

566 Figure 7. $\delta^{13}C$ value of SiC formed by graphite-silicate reaction with degassing of CO
567 and/or CO_2. The initial $\delta^{13}C$ values of graphite (-8.0‰ to -10.7‰) were calculated using
568 the C isotopic compositions of bulk xenoliths (-5.7‰ ~ -8.4‰) based on the C isotope
569 fractionation factor between $CaCO_3$ and graphite (Deines and Eggler, 2009) assuming
570 temperature of 915 °C (Liu et al., 2015). For the detailed modeling method, see Appendix.

This is a preprint, the final version is subject to change, of the American Mineralogist (MSA)
Cite as Authors (Year) Title. American Mineralogist, in press.
(DOI will not work until issue is live.) DOI: http://dx.doi.org/10.2138/am-2017-5721

Appendix

Modeling Method

C isotope compositions of SiC formed by degassing of CO and CO_2 were modeled based on reaction formulas:

$$2C+SiO_2 \rightarrow SiC+CO_2 \quad \text{(Liu et al., 2015)} \tag{S1}$$

$$6C+4MgSiO_3 \rightarrow 2SiC+4CO+2Mg_2SiO_4 \quad \text{(Shiryaev and Gaillard, 2014)} \tag{S2}$$

Because the reactions involve three carbonaceous components, the $\delta^{13}C$ value of SiC cannot be simply calculated using the Rayleigh fractionation formula. Instead, numerical simulation was used to model the C isotope composition of SiC. We divided the reaction into sufficiently short reaction processes in which the C isotope composition of SiC can be readily calculated by

$$R^{SiC} = R^{C} \times \alpha_{SiC/C} \tag{S3}$$

Where R^{SiC} and R^{C} are the C isotope ratio of SiC and graphite, $\alpha_{SiC/C}$ is the C isotope fractionation factor between SiC and graphite. Thus, $\delta^{13}C$ of SiC at every increment i of instantaneous reaction with degassing of CO_2 can be calculated by

$$\begin{cases} \mathrm{R}_{i+1}^{SiC} = \mathrm{R}_{i}^{C} \times \alpha_{SiC/C} \\ \mathrm{R}_{i}^{C} = \frac{\mathrm{R}_{i-1}^{C} - \mathrm{R}_{i}^{SiC} \times (\mathrm{X}/2)/(\mathrm{X}_{i}^{C}) - \mathrm{R}_{i}^{CO_2} \times (\mathrm{X}/2)/(\mathrm{X}_{i}^{C})}{1 - X/(\mathrm{X}_{i}^{C})} \\ \mathrm{R}_{i}^{CO_2} = \mathrm{R}_{i-1}^{C} \times \alpha_{CO_2/C} \\ \mathrm{R}_{i}^{SiC} = \mathrm{R}_{i-1}^{C} \times \alpha_{SiC/C} \end{cases} \tag{S4}$$

and degassing of CO can be calculated by

$$\begin{cases} \mathrm{R}_{i+1}^{SiC} = \mathrm{R}_{i}^{C} \times \alpha_{SiC/C} \\ \mathrm{R}_{i}^{C} = \frac{\mathrm{R}_{i-1}^{C} - \mathrm{R}_{i}^{SiC} \times (\mathrm{X}/3)/(\mathrm{X}_{i}^{C}) - \mathrm{R}_{i}^{CO} \times (2\mathrm{X}/3)/(\mathrm{X}_{i}^{C})}{1 - X/(\mathrm{X}_{i}^{C})} \\ \mathrm{R}_{i}^{CO} = \mathrm{R}_{i-1}^{C} \times \alpha_{CO/C} \\ \mathrm{R}_{i}^{SiC} = \mathrm{R}_{i-1}^{C} \times \alpha_{SiC/C} \end{cases} \tag{S5}$$

This is a preprint, the final version is subject to change, of the American Mineralogist (MSA)
Cite as Authors (Year) Title. American Mineralogist, in press.
(DOI will not work until issue is live.) DOI: http://dx.doi.org/10.2138/am-2017-5721

where R_i^C, $R_i^{CO_2}$, R_i^{CO}, R_i^{SiC} are the C isotope ratio of graphite, CO_2, CO and SiC at stage *i*, respectively. *X* is the graphite consumption molar proportion relative to original graphite (we use *X*=0.001 here), X_i^C is the remnant graphite proportion relative to original graphite at stage *i*. The $\alpha_{SiC/C}$ and $\alpha_{SiC/CO2}$ are the C isotope fractionation factors between SiC and graphite and between SiC and CO_2, respectively. There is no experimental data about $\alpha_{SiC/C}$ and $\alpha_{SiC/CO2}$, therefore, we calculated the fractionation factor through reduced partition function ratios (β-factors) by

$$10^3 ln\alpha_{A/B} = 10^3 ln\beta_A - 10^3 ln\beta_B \text{ (Horita and Polyakov, 2015)} \quad \text{(S6)}$$

Thus $\alpha_{SiC/C}$, $\alpha_{SiC/CO2}$ and $\alpha_{SiC/CO}$ can be expressed by

$$10^3 ln\alpha_{CO_2/C} = 10^3 ln\beta_{CO_2} - 10^3 ln\beta_C \quad \text{(S7)}$$

$$10^3 ln\alpha_{SiC/C} = 10^3 ln\beta_{SiC} - 10^3 ln\beta_C \quad \text{(S8)}$$

$$10^3 ln\alpha_{CO/C} = 10^3 ln\beta_{CO} - 10^3 ln\beta_C \quad \text{(S9)}$$

β_{SiC} is from (Horita and Polyakov, 2015), β_{CO2} and β_{CO} are from (Richet et al., 1977) and β_C is from (Polyakov and Kharlashina, 1995), which are all temperature dependent. Assuming temperatures of 700°C, 900°C, 1100°C and 1300°C, C isotopic compositions of SiC were calculated (Fig. 7).

605 Table 1. Compositions of native metal, silicide, sulfide, Fe-Cr alloy and carbide. The
606 crystallochemical formulas of silicide are calculated by assuming Si as anion and Fe,Ni
607 and Ti as cation. The crystallochemical formulas of sulfide are calculated by assuming S
608 as anion and Fe as cation. The crystallochemical formulas of carbide are calculated by
609 assuming C as anion and Si or Ti as cation.

Sample	Mineral	Si	Ti	Al	Fe	Mn	Ni	Cu	Cr	Total
DLH0601-10	Fe	1.66			99.4	0.38				101.4
DLH06102-20	Fe	1.70	0.02	0.00	99.2	0.34	0.01		0.05	101.4
DLH0601-12	Ni	0.08	0.00	0.00	0.16	0.00	98.7		0.00	98.9
DLH06102-18	Ni				1.54		95.7			97.3
DLH06102-79	Si	98.4	0.00	0.02	0.12		0.01			98.6
DLH06112-3	$(Fe,Ni)_2Si$	19.7			61.1		20.2			100.9
DLH0601-2	$(Fe,Ni)_3Si$	15.5	0.00	0.00	83.6	0.02	0.54		0.16	99.8
DLH06112-5	$(Fe,Ti,Ni)_3Si_7$	53.2	2.42	0.84	43.2		2.62			102.3
DLH0601-07	FeS	0.24			60.7					61.0
DLH0601-11	FeS_2	0.27			45.1					45.6
DLH06102-19	Fe-Cr	0.79		0.20	70.4	0.52	8.10	2.66	16.7	99.4
DLH0601-22	SiC	72.3	0.00	0.00	0.03	0.00	0.00		0.00	72.3
DLH0601-09	TiC	0.04	80.2	0.17	0.02				0.06	80.5

610 Unit is wt% for major elements.

611 Table 2. C-isotope compositions of SiC in DLH06102 analyzed by SIMS.

Number	Analysis Spot	$^{13}C/^{12}C$	Precision[a]	$\delta^{13}C$ (‰)[b]	±2SE	Distance from the edge (μm)
SiC-1	1-1	0.010532	0.17	-18.9	0.35	13.8
SiC-1	1-2	0.010527	0.15	-19.3	0.32	49.3
SiC-1	1-3	0.010532	0.16	-18.9	0.33	75.0
SiC-2	2-1	0.010511	0.30	-20.8	0.63	13.4
SiC-2	2-2	0.010566	0.16	-15.7	0.33	42.5
SiC-2	2-3	0.010585	0.17	-13.9	0.36	74.5
SiC-2	2-4	0.010593	0.16	-13.2	0.32	98.9
SiC-3	3-1	0.010543	0.15	-17.8	0.32	17.9
SiC-3	3-2	0.010551	0.15	-17.1	0.31	40.9
SiC-3	3-3	0.010567	0.16	-15.6	0.33	59.5
SiC-3	3-4	0.010557	0.16	-16.5	0.33	73.9
SiC-4	4-1	0.010505	0.16	-21.4	0.33	18.9
SiC-4	4-2	0.010552	0.16	-17.0	0.33	48.9
SiC-4	4-3	0.010565	0.16	-15.8	0.34	77.9
SiC-5	5-1	0.010490	0.17	-22.8	0.35	1.79
SiC-5	5-2	0.010518	0.16	-20.2	0.32	32.9
SiC-5	5-3	0.010547	0.16	-17.5	0.33	73.2
SiC-6	6-1	0.010564	0.16	-15.9	0.34	5.36
SiC-6	6-2	0.010563	0.16	-16.0	0.33	40.4
SiC-6	6-3	0.010563	0.17	-16.0	0.35	85.2
SiC-7	7-1	0.010515	0.16	-20.5	0.34	99.3

612 [a] Analytical uncertainty in permil (1 σ) for each analysis

613 [b] Values relative to the reference PDB ($^{13}C/^{12}C$=0.0112372) and corrected by the

614 instrumental mass fractionation (0.955) monitored using graphite-1 standard.

This is a preprint, the final version is subject to change, of the American Mineralogist (MSA)
Cite as Authors (Year) Title. American Mineralogist, in press.
(DOI will not work until issue is live.) DOI: http://dx.doi.org/10.2138/am-2017-5721

Figure 1. Tectonic sketch map of the study area modified after Xiao et al. (2003).

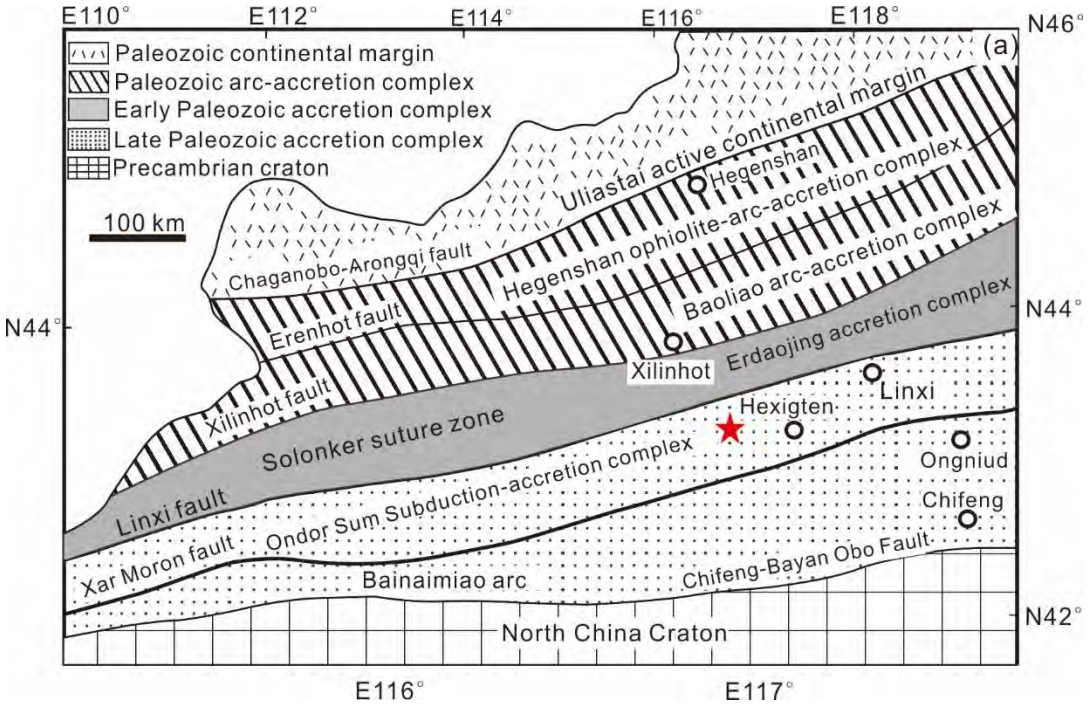

This is a preprint, the final version is subject to change, of the American Mineralogist (MSA)
Cite as Authors (Year) Title. American Mineralogist, in press.
(DOI will not work until issue is live.) DOI: http://dx.doi.org/10.2138/am-2017-5721

Figure 2. **(a)** Field appearance of the carbonatitic xenolith. **(b)** Section of one carbonatitic xenolith. **(c,d)** Pyroxenes in the carbonatitic xenolith.

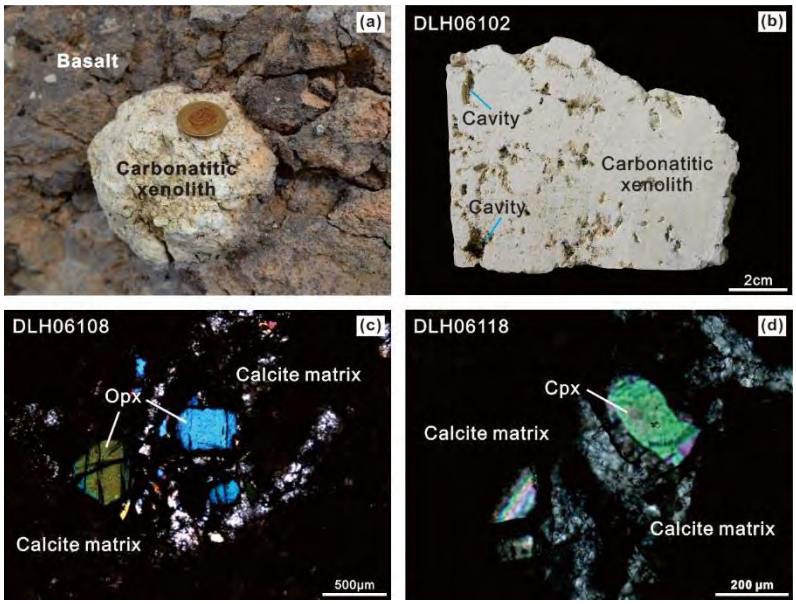

This is a preprint, the final version is subject to change, of the American Mineralogist (MSA)
Cite as Authors (Year) Title. American Mineralogist, in press.
(DOI will not work until issue is live.) DOI: http://dx.doi.org/10.2138/am-2017-5721

Figure 3. **(a)** Optical and **(b)** backscattered electron images of SiC in the micro-cavity. **(c)** Optical image of in-situ graphite in the micro-cavity. **(d)** Backscattered electron image of separated TiC. **(e)** Backscattered electron image of Fe_3Si coexisting with SiC. **(f)** Backscattered electron image of native Ni. **(g)** Backscattered electron image of native Fe. **(h)** Backscattered electron image of feldspar. **(i)** Backscattered electron image of quartz.

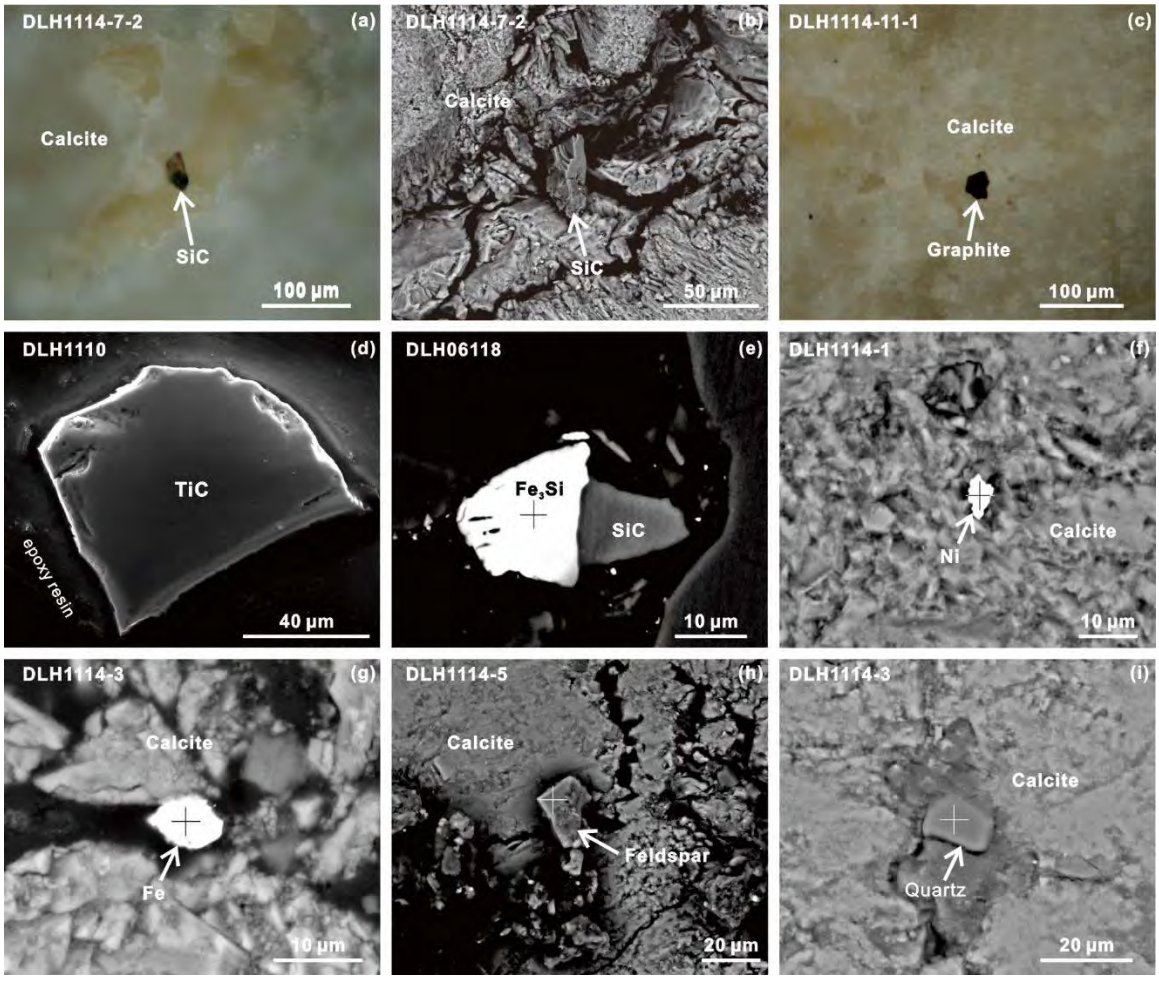

This is a preprint, the final version is subject to change, of the American Mineralogist (MSA)
Cite as Authors (Year) Title. American Mineralogist, in press.
(DOI will not work until issue is live.) DOI: http://dx.doi.org/10.2138/am-2017-5721

Figure 4. Raman spectrums of SiC grains.

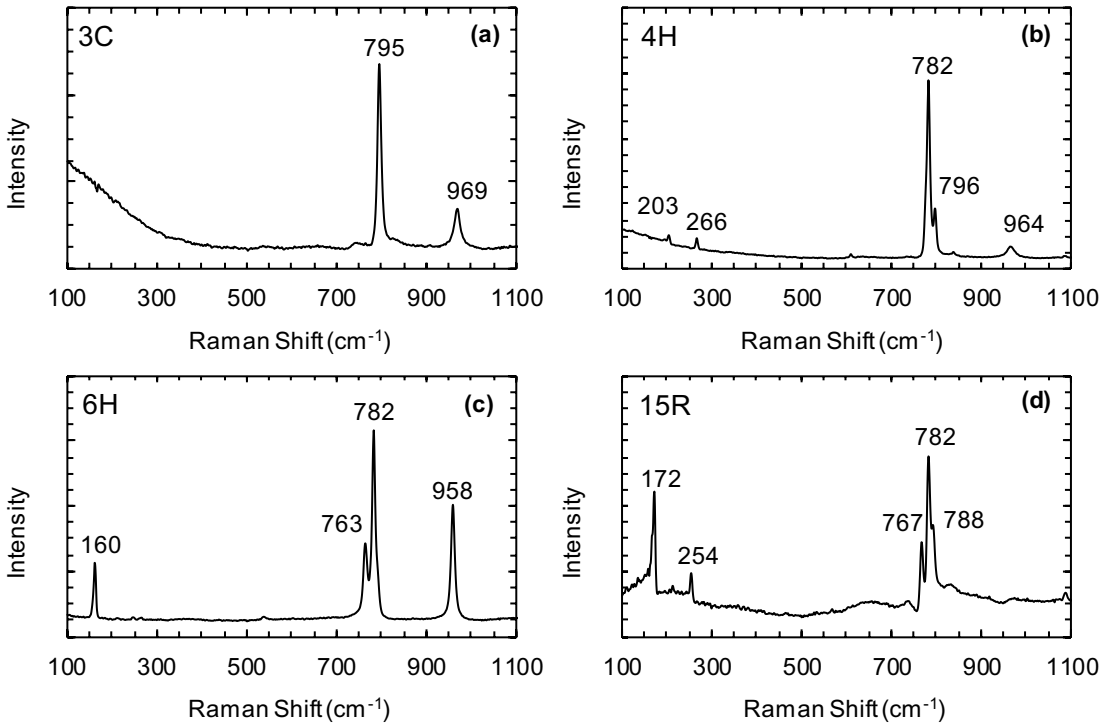

This is a preprint, the final version is subject to change, of the American Mineralogist (MSA)
Cite as Authors (Year) Title. American Mineralogist, in press.
(DOI will not work until issue is live.) DOI: http://dx.doi.org/10.2138/am-2017-5721

Figure 5. Stacked histogram of $\delta^{13}C$ value of SiC from different settings. SiC grains in kimberlite (Mathez et al., 1995), SiC inclusion in diamond (Leung et al., 1990), rock-forming SiC from Turkish beach (Di Pierro et al., 2003; Trumbull et al., 2009) and SiC separated from podiform chromitites from Ray-Iz, Luobusa, Dongqiao and Semail ophiolites (Trumbull et al., 2009) are shown for comparison.

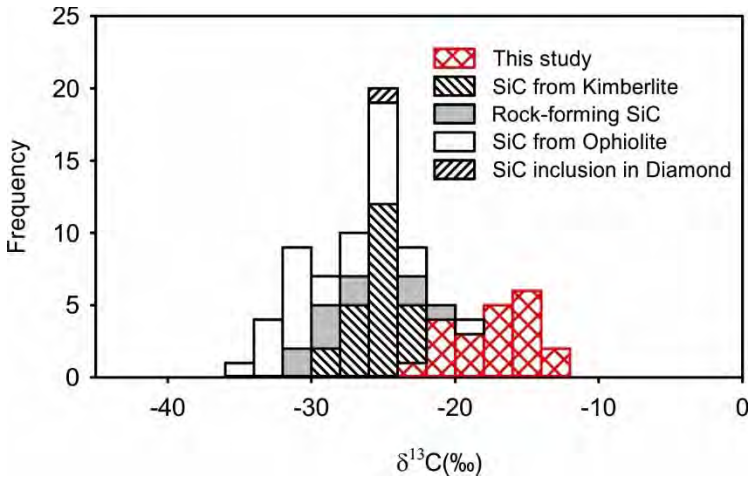

This is a preprint, the final version is subject to change, of the American Mineralogist (MSA)
Cite as Authors (Year) Title. American Mineralogist, in press.
(DOI will not work until issue is live.) DOI: http://dx.doi.org/10.2138/am-2017-5721

Figure 6. Profile variations of $\delta^{13}C$ value of SiC grains. $\delta^{13}C$ value of the bulk carbonatitic xenolith is shown for comparison.

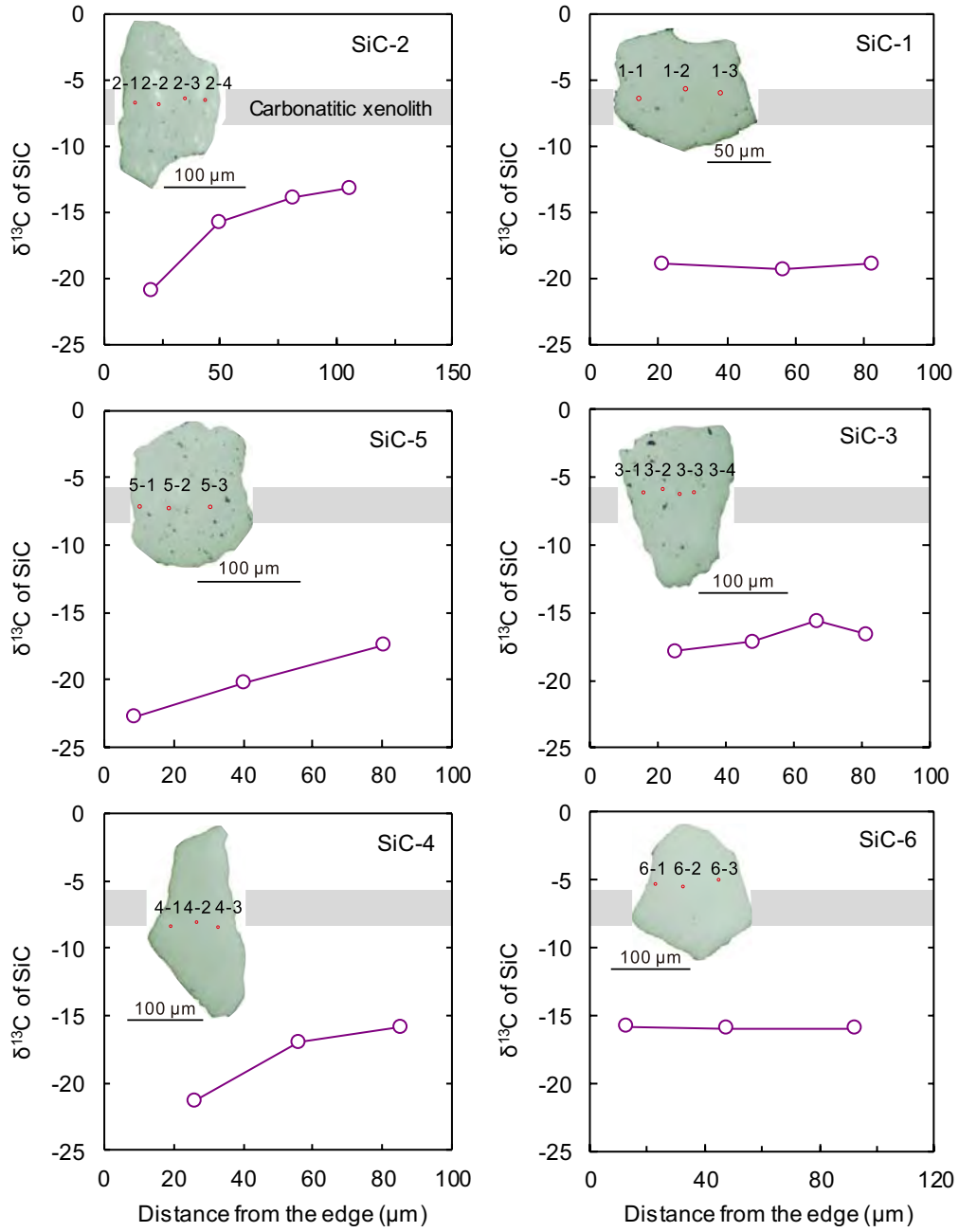

This is a preprint, the final version is subject to change, of the American Mineralogist (MSA)
Cite as Authors (Year) Title. American Mineralogist, in press.
(DOI will not work until issue is live.) DOI: http://dx.doi.org/10.2138/am-2017-5721

Figure 7. $\delta^{13}C$ value of SiC formed by graphite-silicate reaction with degassing of CO and/or CO_2. The initial $\delta^{13}C$ values of graphite (-8.0‰ to -10.7‰) were calculated using the C isotopic compositions of bulk xenoliths (-5.7‰ ~ -8.4‰) based on the C isotope fractionation factor between $CaCO_3$ and graphite (Deines and Eggler, 2009) assuming temperature of 915 °C (Liu et al., 2015). For the detailed modeling method, see Appendix.